Table X. Deviations from the Symmetry Plane of an Idealized C_{2v} Polyhedron[a]

atom	displacement, Å	atom	displacement, Å
O(11)	−1.269 (4)	O(12)	1.313 (4)
O(22)	−0.447 (4)	O(22)′	0.447 (4)

atoms[b]	torsion angle, deg
O(12)′, MID2, MID1, O(11)	2.6
O(11)′, MID2, MID1, O(12)	2.6
O(22), MID2, MID1, O(22)′	19.1

[a] Pseudo symmetry plane formed by atoms Th and O(1) and the point between O(11) and O(12), which yields the plane which is normal to the O(11)–O(12)–O(11)′–O(12)′ least-squares plane. Coordinates of primed atoms are related to the correspondingly numbered atoms of Table III by the C_2 transformation $\bar{x}$, y, $^1/_2 - z$. [b] MID1 and MID2 represent the centroids of the opposing faces formed by [O(11), O(12), O(22)′] and [O(12)′, O(11)′, O(22)].

atively charged NO groups are arrayed symmetrically and are farther apart than would be possible in the C_{4v} geometry. While the larger O–O bite distance of the oxypyridinonate (2.58 Å) compared to tropolonate (2.53 Å) rings may be significant, it seems probable that the asymmetry of the negative charge distribution of the oxypyridinonate compared to tropolonate rings is the major factor in the difference in structure of their nine-coordinate thorium complexes.

Comparison of the effect of ligand-charge asymmetry on Th–O bond length can be made with the structures of the two eight-coordinate hydroxamate complexes of Th^{4+} described earlier. In these aliphatic hydroxamate compounds the Th–O_N bonds are 0.10 and 0.14 Å shorter than the Th–O_C bonds. In the nine-coordinate complex reported here, this difference is less pronounced (~0.07 Å, see Table VII) and thus is consistent with a greater delocalization of charges on this aromatic ring ligand compared with the more localized charge of the simple hydroxamate ligands.

Acknowledgment. This work was supported by the Director, Office of Energy Research, Office of Basic Energy Sciences, Chemical Sciences Division of the U.S. Department of Energy, under Contract No. DE-AC03-76SF00098. We thank Brandan Borgias for his assistance.

Registry No. $(C_5H_4NO_2)_4(H_2O)Th\cdot 2H_2O$, 86728-77-0; $(C_5H_4NO_2)_4Zr$, 86728-75-8; $(C_5H_4NO_2)_4Ce$, 86728-76-9; $(C_5H_4NO_2)_4U$, 86728-78-1.

Supplementary Material Available: Listings of anisotropic thermal parameters (Table IV), idealized hydrogen atom parameters (Table V), observed and calculated structure factor amplitudes (Table VI), and selected least-squares planes (Table VIII) (26 pages). Ordering information is given on any current masthead page.

Contribution No. 3098 from the Central Research and Development Department, Experimental Station, E.I. du Pont de Nemours and Company, Wilmington, Delaware 19898

NMR Spectra of Paramagnetic Group 8 Complexes of Bis(pyridylimino)isoindoline

PETER J. DOMAILLE, RICHARD L. HARLOW, STEVEN D. ITTEL,* and WILLIAM G. PEET

Received January 4, 1983

The susceptibility elements, χ_{ii}, of a series of transition-metal bis(2-pyridylimino)isoindoline (BPI) complexes have been determined by a solution-phase method based upon splittings observed in high-field, high-resolution deuterium NMR spectra. Details of the approach are discussed and applied to the interpretation of chemical shifts in the proton NMR spectra of the $M(BPI)_2$ complexes, M = Fe^{2+}, Co^{2+}, and Ni^{2+}. An X-ray crystal structure of bis(bis(3-methyl-2-pyridylimino)isoindolinato)manganese–methylene chloride (2/1) has been determined and combined with magnetic anisotropy data for the Co^{2+} complex to separate contact and dipolar contributions to the chemical shifts. ESR data and the method of isolated spins are compared with the deuterium quadrupole method of measuring the susceptibility elements in the cobalt complex. The crystal structure data at −100 °C are space group $P\bar{1}$, a = 9.643 (2) Å, b = 38.930 (9) Å, c = 9.539 (2) Å, α = 92.716 (2)°, β = 90.556 (2)°, γ = 86.574 (2)°, and Z = 4 for $Mn(C_{20}H_{16}N_5)_2 \cdot {}^1/_2CH_2Cl_2$, giving two independent molecules. The coordination geometry is octahedral with two meridional, three-coordinate, monoanionic ligands.

Introduction

The interpretation of the NMR spectra of paramagnetic molecules has received considerable attention in recent years.[1] One aspect of continuing focus is the requirement of clearly distinguishing the two independent contributions to the paramagnetic shift, the pseudocontact (dipolar) and contact terms. These individual contributions are separated by calculation of the dipolar shift from eq 1 and subtraction from

$$(\Delta H/H)_D = -\langle(3\cos^2\theta^* - 1)/3R^{*3}\rangle\Delta_\parallel\chi - \langle\sin^2\theta^*\cos 2\phi^*/2R^{*3}\rangle\Delta_\perp \quad (1a)$$

$$\Delta_\parallel\chi = (\chi_{zz} - {}^1/_2(\chi_{xx} + \chi_{yy})) \qquad \Delta_\perp\chi = (\chi_{xx} - \chi_{yy}) \quad (1b)$$

the measured isotropic shift.[1-5] Since a reasonable molecular geometry is usually available, (R^*, θ^*, ϕ^*) are calculable, while the difficult parameters to determine are the susceptibility elements, χ_{ii}.

Horrocks and co-workers[2] pioneered the use of single-crystal anisotropy measurements to determine the χ_{ii} values, while Jesson[3] and McGarvey[4] used low-temperature ESR measurements and ligand field calculations to derive the susceptibility anisotropy ($\Delta_\parallel\chi$) in axial molecules. The former method requires large single crystals with known projections of the molecular axes onto the crystallographic axes, while the latter approach needs detailed information about the excited

(1) (a) LaMar, G. N., Horrocks, W. D., Jr., Holm, R. H., Eds. "NMR of Paramagnetic Molecules"; Academic Press: New York, 1973. (b) Honeybourne, C. L. *Nucl. Magn. Reson. 6–8.*

(2) (a) Horrocks, W. D., Jr. *Inorg. Chem.* **1970**, *9*, 690–692. (b) Horrocks, W. D., Jr. Greenberg, E. S. *Ibid.* **1971**, *10*, 2190.

(3) (a) Jesson, J. P. *J. Chem. Phys.* **1966**, *45*, 1049–1056. (b) Jesson, J. P. *Ibid.* **1967**, *47*, 579–591.

(4) (a) Kurland, R. J.; McGarvey, B. R. *J. Magn. Reson.* **1970**, *2*, 286–301. (b) McGarvey, B. R. *J. Chem. Phys.* **1970**, *53*, 86–91.

(5) The octupolar contributions to the geometry-dependent shift are not expected to be significant in this case since R^* is approximately 5–8 Å for all protons except 6-pyridyl, which is 2.9 Å: (a) Stiles, P. J. *Mol. Phys.* **1975**, *29*, 1271. (b) Golding, R. M.; Pascual, R. O.; Stubbs, L. C. *Ibid.* **1976**, *31*, 1933. (c) Golding, R. M.; Pascual, R. O.; Vrbancich, J. *Ibid.* **1976**, *31*, 731.

0020-1669/83/1322-3944$01.50/0

electronic states[6] and requires estimates of spin–orbit coupling constants and orbital reduction factors. Both methods are also subject to lattice crystalline field effects.

Recently we proposed an alternative solution-phase method to measure χ_{ii} based on splittings observed in a high-field, high-resolution deuterium NMR spectrum.[7] In this paper we present an expanded version of this approach and apply it to the interpretation of chemical shifts in the proton NMR spectra of a series of transition-metal bis(pyridylimino)isoindoline complexes, $M(BPI)_2$; M = Fe^{2+}, Co^{2+}, Ni^{2+}. The numbering scheme for the HBPI ligand is shown below:

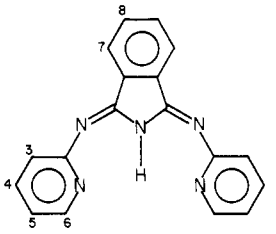

Alkyl substituents have been introduced at the 3-, 4-, and 5-positions.

An X-ray crystal structure of the $Mn(3\text{-MeBPI})_2$ compound has been determined and combined with magnetic anisotropy data for the Co^{2+} complex to separate the contact and dipolar contributions to the chemical shift. ESR data and the method of isolated spins are compared with the deuterium quadrupole method of measuring the susceptibility elements in the Co^{2+} complex.

Results and Discussion

X-ray Structure of $Mn(3\text{-MeBPI})_2$. Since interpretation of the NMR spectra requires that the molecular geometry of the complex is known, an X-ray structure determination was made. The $M(BPI)_2$ complexes, especially the methylpyridyl derivatives, normally precipitate as crystalline solids during synthesis. These crystals are not suitable for X-ray structure determination, so a variety of complexes were recrystallized from a number of solvents. Methylene chloride gave suitable looking crystals of $M(3\text{-MeBPI})_2$ for nickel, cobalt, and manganese, but nickel and cobalt rapidly lost a solvent of crystallization. Therefore, $Mn(3\text{-MeBPI})_2 \cdot {}^1/_2CH_2Cl_2$ was chosen for single-crystal work.

There are two independent molecules (along with one molecule of CH_2Cl_2) in the asymmetric unit. Selected bond distances and angles, which are the averages for the four independent ligand molecules, are shown in Figure 1. A stereoscopic view of one full molecule in shown in Figure 2. Additional perspective and stereoscopic views have been included in the supplementary material.

The structure consists of discrete molecules with no unusual nonbonded interactions. The geometry about the metal center is a distorted octahedron. Coordination of the BPI ligand is very similar to that observed in two copper complexes.[8] Because the two pyridyl groups of a single BPI ligand are unable to fully span the metal, their average trans angle is reduced from 180 to 162.3°. The isoindoline nitrogen atoms are significantly closer to the metal center than the pyridyl nitrogen atoms. This is the same relationship as observed in the Cu complexes,[8] but the larger ionic radius of Mn increases the M–N distances by ~0.25 Å. The average C–C and C–N bond distances of the ligand in the Mn structure agree very closely with those observed in the Cu structures, but the average N–C–N and C–N–C angles of the iminoisoindoline

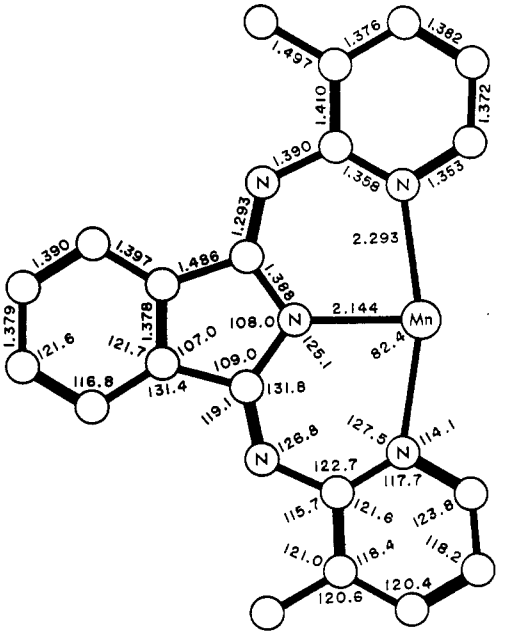

Figure 1. Average bond distances (Å) and angles (deg) for the bis(3-methyl-2-pyridylimino)isoindoline complex of manganese. Errors on the individual structural parameters were ±0.003 Å for the Mn–N distances and ±0.005 Å for the remaining C–C and N–C distances. The N–Mn–N angles had errors of ±0.1° while the remaining (non-hydrogen) angles had errors of ±0.3 or ±0.4°.

portion of the ligand have expanded to accommodate the bulkier metal.

Distortions of the ligands from planarity and away from the axes described by the inner coordination sphere are probably best ascribed to crystal-packing forces. Nonetheless, it is interesting to note several features. The two independent molecules are similar in having one BPI ligand that is relatively planar and another that has one pyridyl group bent well out of the plane. In the planar ligands, the angles between planes defined by the isoindoline groups and the pyridyl groups average 6°. The Mn atoms average over 0.5 Å out of the plane defined by the isoindoline group, and it is evident from the figure that the isoindoline group is bent well off the z axis defined by the inner coordination sphere.

In contrast with the two planar BPI ligands, the two twisted ligands have one pyridyl group coplanar with the isoindoline group and one twisted well out of planarity. This twist is reflected in an average angle of 23° between the isoindoline groups and the twisted pyridyl groups. The isoindoline groups are closer to the z axis of the inner coordination spheres. While the Mn atom averages under 0.4 Å from the isoindoline planes, it is well over 0.6 Å on the opposite side of the plane of the twisted pyridyl group.

It is clear from this structure that while the BPI ligand would be nominally planar to maximize conjugation through its π-system, in the solid it can undergo substantial distortions from planarity. Comparison with the copper BPI structures indicate variability of the chelate size, and variations in the interplanar angles indicate ligand flexibility.

Proton NMR Spectra of Fe^{2+}, Co^{2+}, Ni^{2+}, and Zn^{2+} Complexes. Moderately sharp (~10–500 Hz fwhm) proton NMR spectra were obtained from the paramagnetic Fe^{2+}, Co^{2+}, and Ni^{2+} complexes at room temperature. The line widths are consistent with the order of T_{1e} usually observed,[9] namely, $Co^{2+} < Fe^{2+} < Ni^{2+}$. Assignments were made on the basis of alkyl substitution of the pyridyl ring. The only remaining ambiguity was the distinction between the 7- and 8-positions, which were

(6) Abragam, A.; Pryce, M. L. H. *Proc. R. Soc. London, Ser. A* **1951**, *206*, 173–191.
(7) Domaille, P. J. *J. Am. Chem. Soc.* **1980**, *102*, 5392–5393.
(8) Gagné, R. R.; Gall, R. S.; Lisensky, G. C.; Marsh, R. E. *Inorg. Chem.* **1979**, *18*, 771–781.
(9) Swift, T. J. In ref 1a, pp 53–83.

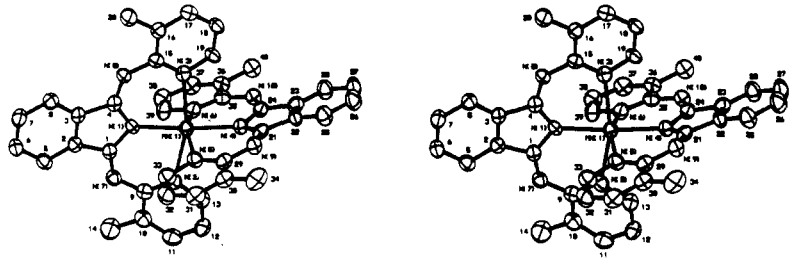

Figure 2. Stereoview of $Mn(3\text{-}MeBPI)_2$ with 50% probability ellipsoids.

Table I. Measured Chemical Shifts (ppm)[a] and Representative Line Widths (Hz) of Fe^{2+}, Co^{2+}, and Ni^{2+} Complexes at 298 K

	position						other
	3	4	5	6	7	8	
$Co(BPI)_2$	−45.3	−0.2	−27.8	−110.3	−37.6	−27.8	
$Co(3\text{-}MeBPI)_2$	...	+3.6	−28.8	−105.0	−39.2	−28.8	−9.12 (CH_3)
$Co(4\text{-}MeBPI)_2$	−44.7	...	−26.5	−108.5	−36.4	−27.2	+16.4 (CH_3)
$Co(5\text{-}MeBPI)_2$	−46.1	+1.3	...	−110.9	−37.1	−27.5	−6.2 (CH_3)
$Co(4\text{-}t\text{-}BuBPI)_2$	−43.1	...	−25.9	−101.0	−36.8	−27.4	+6.3 ($C(CH_3)_3$)
line width	16	...	17	490	18	10	4.5
$Ni(BPI)_2$	−51.5	−12.8	−34.8	...	−12.0	−13.2	
$Ni(3\text{-}MeBPI)_2$	...	−10.9	−37.8	...	−12.7	−13.5	−9.4 (CH_3)
$Ni(4\text{-}MeBPI)_2$	−52.2	...	−33.9	...	−12.5	−13.5	+6.4 (CH_3)
$Ni(5\text{-}MeBPI)_2$[b]	−53.2	−11.6	...	...	−12.0	−13.1	−5.9 (CH_3)
$Ni(4\text{-}t\text{-}BuBPI)_2$	−51.3	...	−33.5	...	−12.5	−13.6	−0.6 ($C(CH_3)_3$)
line width	150	...	140	...	85	50	15
$Fe(BPI)_2$[b]	−41.6	−32.3	−33.9	...	−9.9	−11.5	
$Fe(3\text{-}MeBPI)_2$[b]	...	−29.9	−36.5	...	−9.9	−11.7	−19.4 (CH_3)
$Fe(4\text{-}MeBPI)_2$[b]	−40.8	...	−31.4	...	−9.3	−11.1	+24.2 (CH_3)
$Fe(5\text{-}MeBPI)_2$[b]	−42.2	−29.7	...	...	−9.6	−11.4	−18.0 (CH_3)
$Fe(4\text{-}t\text{-}BuBPI)_2$	−42.1	...	−32.4	...	−9.6	−11.6	−0.6 ($C(CH_3)_3$)
line width	65	...	60	...	40	17	16

[a] In accordance with the sign convention for paramagnetic molecules, negative values represent a shift to lower field at constant frequency. [b] Temperature 315 K.

Table II. Average Isotropic Paramagnetic Shifts (ppm) of Fe^{2+}, Co^{2+}, and Ni^{2+} Complexes at 298 K

	position						
	3	4	5	6	7	8	4-*t*-Bu
$Co(BPI)_2$	−37.9	+7.1	−21.2	−102.3	−29.8	−19.7	+7.5
$Ni(BPI)_2$	−44.8	−3.7	−28.4		−4.7	−5.3	+0.5
$Fe(BPI)_2$	−34.4	−23.3	−27.2		−2.1	−3.5	+0.6
$Zn(BPI)_2$	−7.30	−7.37	−6.67	−8.10	−7.65	−8.12	−1.2
ref shifts					(8.12)	(−7.65)	

not substituted. However, this uncertainty is removed by the considerably broader lines expected for the more strongly dipolar relaxed 7-position. Deuterium NMR confirms this assignment for the Co^{2+} complex (vide infra). Recently Gagné et al.[10] reported a similar assignment for the $M(4\text{-}MeBPI)_2$ derivatives, but the assignment of the 5- and 7-resonances should be interchanged in the case of Co^{2+}. Measured chemical shifts and representative line widths for all assigned peaks are shown in Table I. All six resonances of the Co^{2+} complex are assigned, whereas in Ni^{2+} and Fe^{2+} the pyridyl 6-position is not located because of excessive dipolar broadening.

The spectrum of the diamagnetic Zn^{2+} complex provides a chemical shift reference for removing the inherent diamagnetic contribution from measured paramagnetic shifts, to allow uncontaminated isotropic shifts. Alkyl substitution is again successful in establishing the assignment of all but the 7- and 8-positions, which consist of an AA'BB' multiplet. Gagné[10] has assigned these shifts, but there is no spectroscopic basis for the choice. However, since the two resonances are only separated by 0.5 ppm, an average value is sufficiently accurate in evaluation of the isotropic shifts.

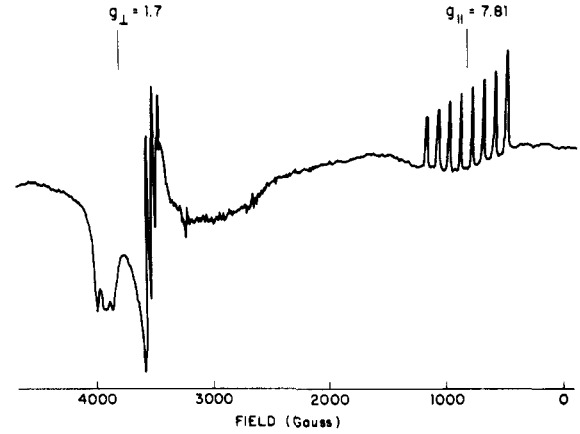

Figure 3. ESR spectrum of a 1/1000 dilute powder of $Co(BPI)_2/Zn(BPI)_2$ at 5 K.

The final average isotropic shifts of the Fe^{2+}, Co^{2+}, and Ni^{2+} complexes are listed in Table II. Since the *tert*-butyl group is expected to have little, if any, spin density, the +7.5 ppm observed shift in Co^{2+} must be ascribed to a dipolar contribution while the relatively minor 0.5 ppm shift is observed in

(10) Gagné, R. R.; Marritt, W. A.; Marks, D. N.; Siegl, W. O. *Inorg. Chem.* **1981**, *20*, 3260–3267.

Table III. Dipolar Shifts, $(\Delta H/H)_D$, and Calculated $\Delta_\parallel\chi$ for Co(4-*t*-BuBPI)$_2$ as a Function of Temperature

$\langle(3\cos^2\theta^* - 1)/R^{*3}\rangle_{4\text{-}t\text{-}Bu} = -2.267 \times 10^{21}$ cm^3

$\langle(\sin^2\theta^*\cos 2\phi^*/R^{*3}\rangle_{4\text{-}t\text{-}Bu} = -2.276 \times 10^{21}$ cm^3

T, K	$(\Delta H/H)_D$, ppm	$10^{26} \times \Delta_\parallel\chi$,[a] cm^3	T, K	$(\Delta H/H)_D$, ppm	$10^{26} \times \Delta_\parallel\chi$,[a] cm^3
223	+11.01	1.46	298	+7.45	0.986
248	+9.81	1.30	323	+6.62	0.876
273	+8.40	1.11			

[a] Conversions: 1.0×10^{-26} cm^3 = 6024.9×10^{-6} cgsu/mol = 6024.9 VVk/mol.

Fe^{2+} and Ni^{2+} suggests dominant contact interactions. Thus, only in the case of the Co^{2+} complex is it necessary to determine the susceptibility elements to separate the contact and pseudocontact contributions to the shifts of the ligand sites. Two conventional approaches were initially used to effect the separation: the low-temperature ESR spectrum and the method of isolated spins.

The ESR spectrum of a 1/1000 dilute powder of Co(BPI)$_2$/Zn(BPI)$_2$ at 5 K is shown in Figure 3. The low-field, hyperfine octet ($I = {}^7/_2$) can be accurately measured to give $g_\parallel = 7.81 \pm 0.02$, $A = 0.0369$ (1) cm^{-1}, while the high-field portion consists of two nearly equal g values with complex, overlapped hyperfine structure. Clearly, in the solid, the molecule has a strong magnetic anisotropy with slight rhombic distortion. We have assumed axial symmetry and estimated an average $g_\perp = 1.7 \pm 0.1$.

At 5 K only the lowest energy Kramers doublet is significantly populated, and the g values in the remaining states have to be calculated. We have followed Jesson's approach[3] of varying the tetragonal distortion and orbital Landē factors in a ligand field calculation to reproduce the experimental ground-stage g values and used the complete theory of Kurland and McGarvey[4] to calculate the susceptibility anisotropy, $\Delta_\parallel\chi$. A wide range of tetragonal distortion parameters (δ) and orbital Landē factors (α', α) fit the measured $g_\parallel - g_\perp$ but only for specific δ, α', and α are the individual $g_\parallel$ and $g_\perp$ satisfactorily fit. Furthermore, the $\Delta_\parallel\chi$ values are essentially constant if the ground-state g values are correctly fit. However, $\Delta_\parallel\chi$ is sensitive to the choice of spin–orbit coupling constant, and we are forced to abandon this approach since optical parameters cannot be determined because of band overlap.

An alternative measure of $\Delta_\parallel\chi$ is obtained by using an empirical approach based on the measured isotropic shift of the *tert*-butyl resonance in Co(4-*t*-BuBPI)$_2$. If we assume axial symmetry, the second term of eq 1a vanishes and $\langle(3\cos^2\theta^* - 1)/R^{*3}\rangle$ over all orientations of the *tert*-butyl group can be evaluated with use of the X-ray skeletal structure. Since the measured shift is expected to be entirely dipolar in nature, $\Delta_\parallel\chi$ may be determined.[11] Additional *tert*-butyl substitution on the indoline ring was attempted so that both $\Delta_\parallel\chi$ and $\Delta_\perp\chi$ could be determined without involving axial symmetry. Unfortunately, the ligand synthesis was unsuccessful. The measured shifts and calculated values of $\Delta_\parallel\chi$ as a function of temperature are reported in Table III. The major uncertainty in this approach is the assumption of axial symmetry, and since the magnitude of $\langle\sin^2\theta^*\cos 2\phi^*/R^{*3}\rangle_{t\text{-}Bu}$ is essentially equal to $\langle(3\cos^2\theta^* - 1)/R^{*3}\rangle_{t\text{-}Bu}$, this may cause substantial error. Furthermore, since the measured isotropic shifts are only of the order of 10 ppm, and the results of the Ni^{2+}, Fe^{2+} measurements suggest uncertainties of 0.5–1 ppm in the assumption of spin isolation, we can only expect an accuracy of 5–10%. These uncertainties favor an independent determination of $\Delta_\parallel\chi$ and $\Delta_\perp\chi$ by high-field deuterium NMR, a procedure we have utilized previously in an axially symmetric case.

(11) This same approach has been employed by other workers. W. D. Horrocks[18] has coined the term "spin-isolated nuclei" to describe the method.

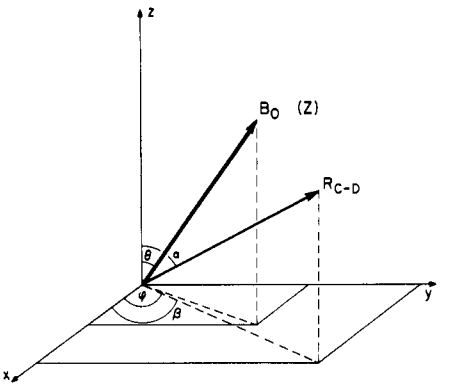

Figure 4. Coordinate system used to describe the principal susceptibility axes (x, y, and z), the C–D bond direction defined by polar angles (α and β), and the orientation of the molecule at polar angles (θ and ϕ) to an external magnetic field B_0.

Susceptibility Measurements Using High-Field Deuterium NMR. The concept of using high-resolution deuterium NMR to measure the susceptibility tensor bears a strong similarity to the use of nematic liquid-crystal solvents[12] as orienting media, where the quadrupole coupling interaction ($I > 1$) is not averaged to zero, and a splitting of lines occurs. In our case, orientation is achieved by placing a solution of the magnetically anisotropic molecule in a strong magnetic field. The degree of orientation, and hence the magnitude of the splitting, is proportional to the susceptibility elements of the solute.

Figure 4 shows the axis systems used to describe the effect. A molecule with principal susceptibility axes (x, y, z) has an internal C–D bond directed at polar angles (α, β), and the molecule itself is oriented at polar angles (θ, ϕ) to an external magnetic field, B_0, directed along the space-fixed Z axis. If we assume the C–D bond to have axial symmetry, the first-order quadrupolar correction to the Zeeman energy is[13]

$$E_m(Q) = (e^2qQ/h)\langle(3\cos^2\gamma - 1)/2\rangle \times [3m^2 - I(I+1)]/[4I(2I-1)] \quad (2)$$

where γ is the angle between the C–D vector and the static field. Since the C–D axis is fixed in the molecule, the average $\langle(3\cos^2\gamma - 1)/2\rangle$ depends on geometric functions of α and β and ensemble averages of functions of θ and ϕ. The average in eq 2 is

$$\langle(3\cos^2\gamma - 1)/2\rangle = \langle(3\cos^2\theta - 1)/2\rangle \times (3\cos^2\alpha - 1)/2 + \langle\sin^2\theta\cos 2\phi\rangle(3\sin^2\alpha\cos 2\beta)/4 \quad (3)$$

The averages over θ and ϕ reflect the competition between the alignment tendency of the field and the randomizing Brownian motion. The magnetic interaction energy is[14]

$$E = (-B_0^2/2)\sum_{g=x,y,z}\chi_{gg}l_{Zg}^2 \quad (4)$$

where l_{Zg} is the direction cosine between the space-fixed Z axis and the molecule-fixed g axis. From Figure 4

$$E(\theta,\phi) = -B_0^2[\chi_{xx}\sin^2\theta\cos^2\phi + \chi_{yy}\sin^2\theta\sin^2\phi + \chi_{zz}\cos^2\theta]/2 \quad (5)$$

(12) Diehl, P.; Khetrapal, C. L. *NMR: Basic Princ. Prog.* **1969**, *1*, 1–95.
(13) Schlichter, C. P. "Principles of Magnetic Resonance"; Harper and Row: New York, 1963; pp 172–174.
(14) Gordy, W.; Cook, R. L. "Microwave Molecular Spectra"; Interscience: New York, 1970; p 383.

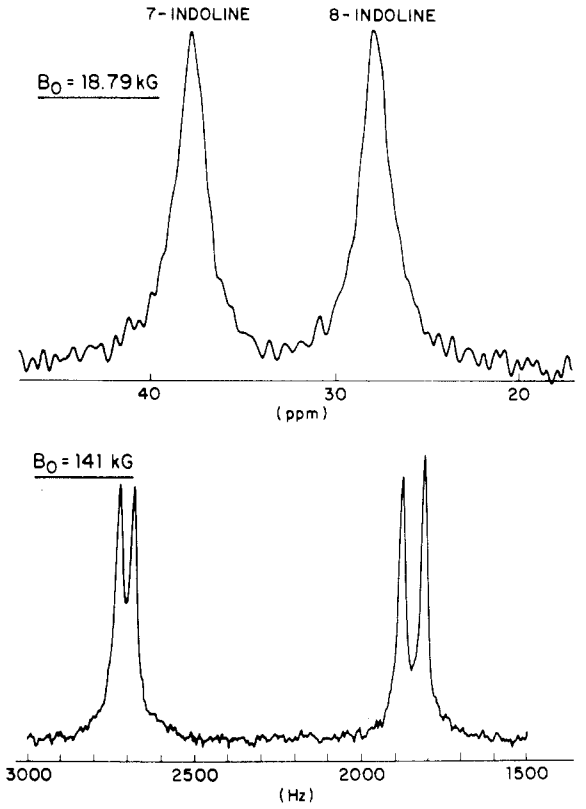

Figure 5. Deuterium NMR spectra of Co(4-MeBPI-d_4)$_2$ at 18.79 and 141 kG.

The averages in eq 3 are evaluated from eq 5 and Boltzmann statistics with $E(\theta,\phi)/kT \ll 1$ to give

$$\langle(3\cos^2\theta - 1)/2\rangle = \Delta_{\parallel}\chi B_0^2/15kT \quad (6a)$$

$$\langle\sin^2\theta\cos 2\phi\rangle = \Delta_{\perp}\chi B_0^2/15kT \quad (6b)$$

In accordance with intuition, eq 6a describes the magnetic alignment as proportional to the magnetic anisotropy, $\Delta_{\parallel}\chi$, while eq 6b reflects the rhombic distortion from magnetic axial symmetry, $\Delta_{\perp}\chi$. MacLean and co-workers[15] have derived identical equations in their recent work of diamagnetic susceptibility anisotropy measurements of polyaromatics.

Equations 6a, 6b, and 3 may be substituted into eq 2 to give the residual quadrupolar splitting of an $I = 1$ nucleus as

$$\Delta\nu_Q = [(e^2qQ/h)B_0^2/20kT][(3\cos^2\alpha - 1)\Delta_{\parallel}\chi + ((3\sin^2\alpha\cos 2\beta)/2)\Delta_{\perp}\chi] \quad (7)$$

Thus, measured quadrupolar splittings of deuterons with known α and B can be used to evaluate $\Delta_{\parallel}\chi$ and $\Delta_{\perp}\chi$. Note that the splittings are independent of distance of the deuterons from the paramagnetic center so that molecular symmetry is sufficient to estimate the angles. Since the degree of alignment is quadratic in the field,[7] the effects are most apparent at the high fields available with superconducting magnets.

Deuterium NMR Spectra of Co(BPI)$_2$ Complexes. The deuterium NMR spectrum of Co(4-MeBPI-d_4)$_2$[16] at 141 kG is shown in Figure 5. Each indoline resonance is clearly split whereas at 18.8 kG they both appear as single Lorentzian lines.

Table IV. Observed and Calculated Quadrupolar Splittings from Weighted Least Squares to Fit $\Delta_{\parallel}\chi$ and $\Delta_{\perp}\chi$

site	$\Delta\nu_Q$, Hz obsd	$\Delta\nu_Q$, Hz calcd[a]	$\Delta\nu_Q$, Hz calcd from jump model[b]
3-pyridyl	70.6 ± 2	61.3 ± 2	61.6
4-pyridyl	−45.5 ± 2	−40.7 ± 4	−39.3
5-pyridyl	72.1 ± 1	74.2 ± 3	74.3
6-pyridyl	46 ± 8	58.4 ± 2	58.6
7-indoline	−41.4 ± 1	−42.4 ± 4	
8-indoline	67.0 ± 1	66.8 ± 2	

$\Delta_{\parallel}\chi = 1.146\ (28) \times 10^{-26}$ cm^3; $\Delta_{\perp}\chi = -1.42\ (36) \times 10^{-27}$ cm^3
$\beta = 90°$

[a] The quadrupole coupling constant of the pyridyl deuterons was taken to be the same as that of pyridine-d_5 (180 kHz) while the constant for the indoline deuterons was assumed to be the same as that of benzene-d_6 (185 kHz). [b] For symmetric jump model of ±20° (see text).

Measured splittings are ±41.4 and ±67.0 Hz for the 7- and 8-positions, respectively.

The inner coordination geometry is expected to be of D_{2d} symmetry with the S_4 axis as the unique z principal susceptibility axis. Distortions in the crystal structure are attributed to lattice-packing effects. The splitting of the 8-indoline (α = 30°) resonance should then be 1.25 times larger than that of the 7-position (α = 90°) for equal quadrupole couplings. Since the measured ratio is 1.62, the molecule must be magnetically nonaxial with a non-zero second term in eq 7. Alternatively, the measured splitting is an average, arising from different rapidly exchanging structures. Both possibilities were examined in an attempt to resolve the difference.

In a nonaxial molecule the x and y axes can be located by measuring splittings of sites with different β values. If the BPI ligand is planar, only the product of (cos 2β)$\Delta_{\perp}\chi$ can be determined since all β values are the same. For example, the measured values for the 7- and 8-positions can be solved to give $\Delta_{\parallel}\chi = 1.135 \times 10^{-26}$ cm^3 and (cos 2β)$\Delta_{\perp}\chi = 1.49 \times 10^{-27}$ cm^3. Note that the *minimum* $\Delta_{\perp}\chi$ is 13% of $\Delta_{\parallel}\chi$, confirming the premise of considerable error in the *tert*-butyl spin isolation approach, which is based on axial symmetry.

Location of the x and y axes was attempted from the high-field deuterium NMR spectrum of Co(BPI-d_8),[16] in which deviation of the pyridyl ring from coplanarity with the indoline would produce different β values for the various sites. All four pyridyl resonances split at 141 kG; the measured splittings and estimated uncertainities are listed in Table IV. With use of the average geometry of Figure 1, the six independent quadrupole splittings were fit by least squares to obtain $\Delta_{\parallel}\chi$ and $\Delta_{\perp}\chi$. A systematic variation of the pyridyl plane dihedral angle produced worse fits than a planar ligand structure. Thus, no statistical change is caused by varying β, and the x and y axes are not located. Table IV compares the observed and fitted values for a planar ligand. Given the uncertainties associated with estimating the structure, the fit is remarkably good. The inherent contradiction in the fit is that two orthogonal planar BPI ligands would constitute axial symmetry with $\Delta_{\perp}\chi = 0$. Nonrigidity and model limitations probably account for this dichotomy.

If the measured splittings are the result of a fast exchange averaged susceptibility tensor, *or* C–D vector, the problem cannot be solved because of the limited data. An estimate of the magnitude of motional effects is possible by forcing the two indoline splittings to fit a two-site axial model, that is, assuming the C–D bonds rotate relative to the $\chi_{\parallel}$ axis. The measured ratio of 1.62 can be obtained with jumps of ±20° and give $\Delta_{\parallel}\chi = 1.39 \times 10^{-26}$ cm^3. This same motion produces calculated values for the four pyridyl sites that are indistinguishable from those of the earlier nonaxial model (Table IV).

(15) (a) Lohman, J. A. B.,; MacLean, C. *Chem. Phys.* **1978**, *35*, 269–274; **1979**, *43*, 144. (b) Lohman, J. A. B.; MacLean, C. *Chem. Phys. Lett.* **1978**, *58*, 483–486; **1979**, *65*, 617. (c) Lohman, J. A. B.; MacLean, C. *Mol. Phys.* **1979**, *38*, 1255–1261. (d) Lohman, J. A. B.; MacLean, C. *J. Magn. Reson.* **1981**, *42*, 5–13.

(16) In Co(4-MeBPI-d_4)$_2$ the two pairs of equivalent sites on the indoline moiety are deuterated whereas in Co(BPI-d_8)$_2$ the four pyridyl sites are substituted.

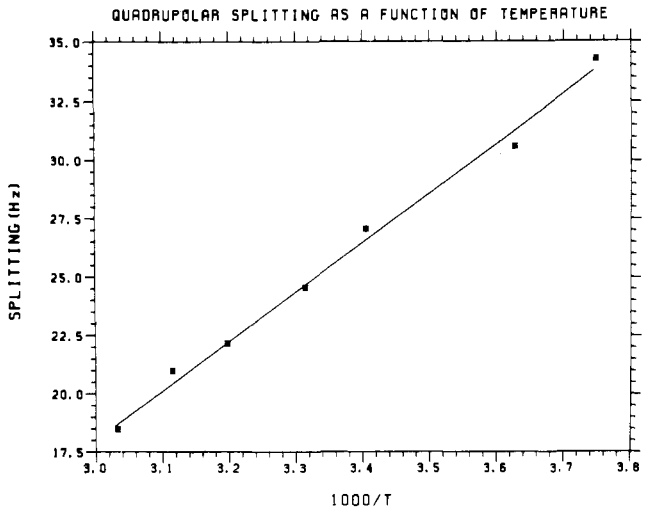

Figure 6. Splittings (Hz) of the 5-pyridyl resonance of $Co(BPI)_2$ as a function of temperature.

Our attempts to obtain *both* $\Delta_\parallel\chi$ and $\Delta_\perp\chi$ from our solution-phase measurements are thus of dubious merit. The most significant conclusion is that the molecular geometry of $Co(BPI)_2$ in solution closely parallels that of $Mn(BPI)_2$ in the solid and that the magnetic anisotropy $\Delta_\parallel\chi$ is comparable with that from the spin-isolation approach and from ligand field calculations.

It is worthwhile reiterating the approximations inherent in using deuterium NMR to measure the components of the molecular susceptibility tensor. First, the molecule must be rigid (with at least a C_2 axis of symmetry) with known C–D angles relative to the principal susceptibility axis. The deuterium quadrupole coupling constant must be known and is assumed to have no asymmetry. Enough sites must be deuterated so that the number of observables, with sufficiently different α and β values, exceeds the number of unknowns. Localized magnetic anisotropy, such as that from an aromatic ring, is neglected. If all of these criteria are not met, the result will be of limited accuracy.

Our current failure to obtain a unique solution may be due to more than one of the above reasons. However, we have continued the analysis and used the derived $\Delta_\parallel\chi$ and the *minimum* possible $\Delta_\perp\chi$ ($\cos 2\beta = -1$). This approach may be partially justified because the $\Delta_\parallel\chi$ value derived from the spin-isolation approach is about 14% lower than that of the deuterium quadrupole approach. The former method forces axial symmetry and will fold the effect of any $\Delta_\perp\chi$ into $\Delta_\parallel\chi$ since the geometric averages (Table III) are very similar. Use of the full eq 1 would significantly reduce the difference between the two results.

The temperature dependence of the splittings was determined at 85 kG over the range 267–330 K; the only resonances clearly split over the entire range were the 3-pyridyl and 5-pyridyl deuterons. A plot of the 5-pyridyl splitting as a function of $1/T$ is shown in Figure 6. Unfortunately, the two equations describing the splitting of the 3- and 5-sites are almost linearly dependent since α is very similar. Thus $\Delta_\parallel\chi$ and $\Delta_\perp\chi$ are not accurately determined, as they were in the previous 141-kG spectra. If we assume that the *relative* values of $\Delta_\parallel\chi$ and $\Delta_\perp\chi$ do not vary with temperature, the data of Figure 6 and the previous $\Delta_\parallel\chi(293)$ and $\Delta_\perp\chi(293)$ values can be used to give $\Delta_\parallel\chi$ and $\Delta_\perp\chi$ as a function of temperature. A more satisfying solution to this problem awaits variable-temperature capabilities at higher field to give more measured splittings for least-squares analysis.

Pseudocontact and Contact Shift Separation: Calculation of Spin Densities. With use of the basic skeletal geometry of the $Mn(3\text{-MeBPI})_2$ complex and the $\Delta_\parallel\chi$ and $\Delta_\perp\chi$ from the deuterium NMR measurements, the dipolar contribution to the chemical shift of $Co(BPI)_2$ can be calculated and subtracted from the measured isotropic shift to give the contact shift. These data are collected in Table V for $T = 298$ K. The variable-temperature data are presented graphically in Figure 7, where the resultant contact shift of the pyridyl sites of the Co^{2+} complex are compared with the corresponding shifts in the Ni^{2+} complex. The close similarity of the plots is gratifying since the ratios of contact shifts are expected to be essentially constant because ligand MO coefficients are only slightly affected[2a] by a change of the central metal ion.

Table V. Separation of Contact and Dipolar Shifts (ppm) in $Co(BPI)_2$ at 298 K

position	$\Delta H/H$ measd	dipolar	contact
3-H	−37.86	+7.77	−45.63
4-H	+7.10	+13.63	−6.53
5-H	−21.16	+10.26	−31.42
6-H	−102.3	−46.30	−56.00
7-H	−29.83	−24.67	−5.16
8-H	−19.67	−15.06	−4.61

$\Delta_\parallel\chi = 1.111 \times 10^{-26}$ cm^3; $\Delta_\perp\chi = -0.136 \times 10^{-26}$ cm^3

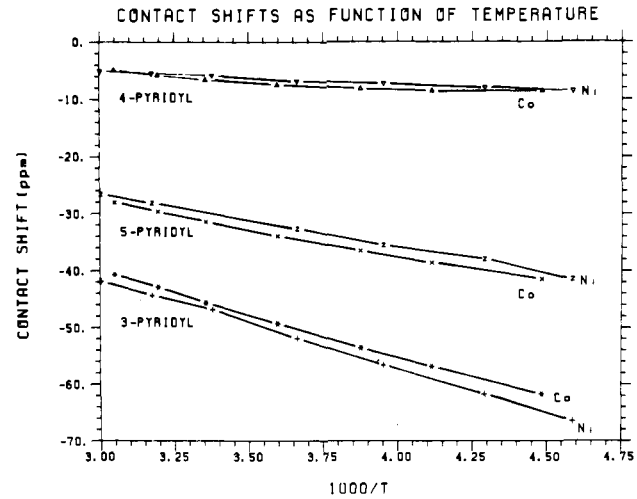

Figure 7. Temperature dependence of contact shifts of the pyridyl resonances of $Co(BPI)_2$ and $Ni(BPI)_2$.

The contact shift of the Co^{2+} complex can be used to compute the hyperfine constants by using the complete theory of McGarvey,[4b] which includes both the g-value anisotropy (F_1) and second-order Zeeman (F_2) terms. For this purpose, it is necessary to resort to the ligand field calculations, which were abandoned in calculating $\Delta_\parallel\chi$ and $\Delta_\perp\chi$. Fortunately F_1 and F_2 are insensitive to sensible ranges of parameter adjustment. Contact densities were calculated from the McConnell relation.[17]

The hyperfine constants for the Ni^{2+} and Fe^{2+} complexes were calculated from the Bloembergen–McConnell formula[18] with use of values of the magnetic moment derived from the Evans[19] method. The hyperfine constants and contact densities for Co^{2+}, Ni^{2+}, and Fe^{2+} are collected in Table VI.

It is tempting to speculate on the mechanism of spin delocalization to rationalize the observed spin densities and perhaps explain the alternation in ligand bond lengths. However, the magnitudes are small and, in the absence of all valence electron MO calculations, only the trends are noted. The smallest spin densities are furthest from the metal coordination site and for

(17) McConnell, H. M. *J. Chem. Phys.* **1956**, *24*, 764.
(18) (a) McConnell, H. M.; Chestnut, D. B. *J. Chem. Phys.* **1958**, *28*, 107. (b) Bloembergen, N. *Ibid.* **1957**, *27*, 595.
(19) Evans, D. F. *J. Chem. Soc.* **1959**, 2003.

Table VI. Hyperfine Constants (A_H) and Spin Densities (ρ_C) in $Fe(BPI)_2$, $Co(BPI)_2$, and $Ni(BPI)_2$

site	A_H, MHz			$10^3\rho_C$		
	Fe	Co	Ni	Fe	Co	Ni
3-pyridyl	0.17	0.30	0.57	−2.7	−4.7	−9.0
4-pyridyl	0.12	0.04	0.05	−1.8	−0.7	−0.7
5-pyridyl	0.13	0.20	0.36	−2.1	−3.2	−5.7
6-pyridyl		0.36			−5.8	
7-indoline	0.01	0.03	0.06	−0.2	−0.5	−1.0
8-indoline	0.02	0.03	0.07	−0.3	−0.5	−1.1

the pyridyl ring $\rho_3 \approx \rho_6 > \rho_5 > \rho_4$. This attenuation with distance is indicative of σ spin delocalization. On the other hand, methyl substitution at the 4-position produces shifts of sign opposite to that of the protonated derivative, a phenomenon usually taken as diagnostic of π spin delocalization. Almost certainly both types of ligand MO's are involved in the complexation and, with the definition of σ or π type delocalization becoming poorly defined in nonplanar systems, no clear distinction is possible.

Experimental Section

The highest field deuterium NMR spectra were recorded at Carnegie-Mellon University at 140.96-kG, providing a deuterium resonance frequency of 92.14 MHz. Spectra were restricted to 293 K. Variable-temperature, high-field deuterium spectra were obtained at the Middle Atlantic Regional Facility on a Bruker WH-360 operating at a frequency of 55.5 MHz. Low-field deuterium spectra and all proton spectra were recorded on a Bruker HFX-90 with a Digilab FTS/NMR-3 Data System. All spectra were recorded as chloroform or chloroform-d_1 solutions.

Initial syntheses of the various BPI free ligands and metal BPI complexes were carried out according to the procedures of Siegl.[20] The long reflux times and overall yields of 50–80% prompted us to seek more convenient higher yield reactions.[21] Similar procedures have been reported elsewhere.[22] Several typical syntheses are described:

[Co(3-MeBPI)$_2$]. Method A. A glass flask equipped with a mechanical stirrer and condenser was charged with 1,2-dicyanobenzene (30 g, 0.23 mol) and 2-amino-3-methylpyridine (50.64 g, 0.468 mol). The flask was placed in an oil bath, which was then heated to 210 °C for 3 h (reaction temperature 194–196 °C). Measurement of ammonia evolution indicated that conversion to H-3-MeBPI ceased after 3 h. At this point, NMR indicated greater than 80% conversion to H-3-MeBPI.

After the mixture was cooled to ambient temperature, 75 mL of toluene was added to the product to improve stirring. The temperature was then increased to 90 °C, and sodium hydroxide (9.36 g, 0.23 mol) in methanol (45 mL) was added. Cobalt acetate (28.57 g, 0.12 mol) was then added in one portion to the resulting slurry in 300 mL of methanol. The resulting brick red slurry was heated for 1 h. The mixture was cooled to 40 °C, and the $Co(3\text{-}MeBPI)_2$ was separated by filtration through a coarse-porosity fritted-disc funnel and washed with 300 mL of methanol followed by 150 mL of diethyl ether to facilitate drying. The yield of analytically pure $Co(3\text{-}MeBPI)_2$ was 78.4 g (96%).

Method B. A 15-gal stainless steel Pfaulder vessel was equipped with a glass water-cooled condenser. The vessel was jacketed to provide heat and cooling via circulating oil. Agitation was provided with a stainless steel paddle with rubber scraper, which was powered with an electric motor. The vessel was charged with 1,2-dicyanobenzene (1680 g, 13.1 mol) and 2-amino-3-picoline (2835 g, 26.2 mol) and then heated to 210 °C for 4 h after the vessel was at temperature. The resulting yellow melt was stirred at 60 rpm. Ammonia evolved during the reaction was scrubbed with water. After 4 h the green melt was cooled to 120 °C, and 4.2 L of toluene was added over 1 min. Sodium hydroxide (524.44 g, 13.1 mol) in 2.52 L of methanol was then added (over 1 min) to this green slurry. After an additional 5 min of stirring, a solution of cobalt acetate (1633 g, 6.56 mol) was added in 16.8 L of methanol. The addition was complete in 10 min to yield a brick red precipitate of $Co(3\text{-}MeBPI)_2$. The reaction was then stirred for an additional 45 min while the vessel was cooled to 40 °C. The $Co(3\text{-}MeBPI)_2$ was then collected by filtration through cotton duck. The filtration was complete in 10 min. The product was washed with 9 L of methanol and then dried in vacuo at 80 °C: yield 4.67 kg (theoretical 4.67 kg); total time, 7 h.

2-Amino-4-*tert*-butylpyridine and Related Compounds. Dimethylaniline (266 g), *tert*-butylpyridine (135 g, 1 mol), and $NaNH_2$ (46 g, 1.18 mol) were combined under a nitrogen atmosphere. The mixture was heated to 150 °C for 6 h, cooled, and carefully poured into 400 mL of ice water. The mixture was filtered through a medium frit, and then the dimethylaniline layer was separated and dried over $CaCl_2$. Dimethylaniline was removed on a rotary evaporator at 60 °C. At this point, the results were highly variable, even for reactions run side by side under identical conditions, and the procedure varied accordingly. If white crystals deposited from a yellow oil, they were collected by filtration. This material was identified as 4,4′-di-*tert*-butyl-3,3′-bipyridyl (**1**). The viscous oil that remained was placed in a sublimer and sublimed onto a −78 °C cold finger over 1 week, giving a yellow solid. A resublimation gave a white product identified as 2-amino-4-*tert*-butylpyridine (**2**). A final extraction of the remaining residue with pentane gave more of the bipyridyl product. The remaining black tar was taken up in ether and treated with Darco to give a yellow-brown solution. Addition of hexane caused precipitation of a yellow product identified as 2,2′-diamino-4,4′-di-*tert*-butyl-5,5′-bipyridyl (**3**). Total products from the reaction gave a combined yield of up to 50%. The highest yield of the desired monomeric product was ~30%.

NMR (assignment (resonance in ppm, intensity, coupling in Hz)): **1**, H_6 (8.55, 2, d of d, J = 0.7, 5.2), H_2 (8.44, 2, d of d, J = 0.7, 2.0), H_5 (7.30, 2, d of d, J = 2.0, 5.2), *t*-Bu (1.37, 18, s); **2**, H_6 (7.96, 1, d of d, J = 0.7, 5.5), H_5 (6.65, 1, d of d, J = 1.6, 5.5), H_3 (6.46, 1, d of d, J = 1.6, 0.7), NH_2 (4.15, 2, broad), *t*-Bu (1.35, 9, s).

H4-*t*-BuBPI. A solution of phthalonitrile (9.0 g, 70 mmol), 2-amino-4-*tert*-butylpyridine (23.1 g, 154 mmol), and $CaCl_2$ (1 g, 9 mmol) were refluxed in *n*-butanol (150 mL) for 3 days. The mixture was cooled to room temperature. The filtrate was stripped to dryness on the vacuum line, yielding a crude material containing 4-*t*-BuBPI and 4-*t*-Bu-2-NH_2py. The excess aminopyridine was sublimed out of the mixture. The product was then recrystallized from methylene chloride; yield 22 g, 76%.

Co(4-*t*-BuBPI)$_2$. A solution of 4-*t*-BuBPI (2.05 g, 5 mmol) in methanol (30 mL) was treated with NaOH (0.20 g, 5.0 mmol). The mixture was heated to dissolve the NaOH. A solution of $CoCl_2 \cdot 6H_2O$ (0.60 g, 2.5 mmol) in methanol was added, giving an immediate brick red crystalline product. The mixture was stirred 2 h and then collected by vacuum filtration. The product was dried under vacuum.

4-*tert*-Butylphthalic Acid. 4-*tert*-butyl-*o*-xylene (40 g) was suspended in 1500 mL of water with vigorous stirring. The mixture was brought to reflux, and a total of 110 g of potassium permanganate was added over a period of 20 h. The mixture was cooled, and 8 g of NaOH was added. The suspension was filtered through Celite and then concentrated to ~115 mL. HCl was added to the solution until the pH was below 5, which caused white solids to precipitate. The solids were recrystallized from ether/hexane: yield 24.4 g; mp 154 °C.

4-*tert*-Butylphthalonitrile. A suspension of *tert*-butylphthalic acid (14 g, 63 mmol) in chlorobenzene (100 mL) was treated with concentrated NH_4OH (20 mL, 300 mmol). The mixture was warmed slowly to 65 °C for 2 h and then taken to reflux. The excess NH_3 and H_2O were azeotroped off. When no more water was coming off, the mixture was cooled to 65 °C and pyridine (10.5 g, 133 mmol) was added. $P(O)Cl_3$ (20.4 g, 133 mmol) was added dropwise over 15 min. After addition was complete, the mixture was maintained at 75 °C for 2 h. The mixture was then cooled to 0 °C, and ice and water were added with caution. After addition of 100 mL of water, the mixture was filtered and the organic layer was stripped to a viscous oil. The oil was taken up in ether (20 mL), and addition of pentane caused the oil to separate. Removal of pentane and ether under vacuum caused the oil to crystallize.

2-Aminopyridine-d_4. An attempt to prepare the deuterated aminopyridine from pyridine-d_5 and $NaNH_2$ resulted in the desired

(20) Siegl, W. O. *J. Org. Chem.* **1977**, *42*, 1872; *Inorg. Nucl. Chem. Lett.* **1974**, *10*, 825.
(21) (a) Druliner, J. D.; Ittel, S. D.; Krusic, P. J.; Tolman, C. A. U.S. Patent 4 326 084, 1982; Eur. Pat. Appl. 80 106 169.8, June 5, 1981. (b) Ittel, S. D.; Peet, W. G. Eur. Pat. Appl. 81 107 301, March 24, 1982; *Chem. Abstr.* **1982**, *97*, (19), 162826*d*.
(22) Addison, A. W.; Burke, P. J. *J. Heterocycl. Chem.* **1981**, *18*, 803.

Table VII. Positional Parameters and Their Estimated Standard Deviations[a]

atom	x	y	z	B, Å²	atom	x	y	z	B, Å²
Mn(1)	0.02571 (8)	0.61543 (2)	0.38673 (8)	2.56 (2)	C(30)	−0.0236 (5)	0.5471 (1)	0.7624 (5)	3.3 (1)
Mn(2)	0.10240 (8)	0.11589 (2)	0.06913 (8)	2.58 (2)	C(31)	−0.1234 (6)	0.5660 (1)	0.8378 (5)	3.9 (1)
Cl(1)	0.2873 (2)	0.25442 (6)	−0.0013 (2)	8.31 (6)	C(32)	−0.1834 (6)	0.5960 (1)	0.7868 (6)	4.1 (1)
Cl(2)	0.5035 (2)	0.23344 (6)	−0.2010 (2)	8.44 (6)	C(33)	−0.1377 (5)	0.6064 (1)	0.6608 (5)	3.6 (1)
N(1)	−0.0572 (4)	0.66636 (9)	0.4488 (4)	2.46 (9)	C(34)	0.0439 (7)	0.5146 (1)	0.8184 (6)	4.9 (2)
N(2)	−0.1979 (4)	0.6096 (1)	0.3124 (4)	3.0 (1)	C(35)	0.1488 (5)	0.6039 (1)	0.0658 (5)	2.8 (1)
N(3)	0.2306 (4)	0.6373 (1)	0.4728 (4)	2.71 (9)	C(36)	0.1732 (5)	0.6144 (1)	−0.0715 (5)	2.8 (1)
N(4)	0.1236 (4)	0.56570 (9)	0.3351 (4)	2.46 (9)	C(37)	0.1059 (6)	0.6444 (1)	−0.1138 (5)	3.5 (1)
N(5)	−0.0381 (4)	0.5889 (1)	0.5839 (4)	2.9 (1)	C(38)	0.0209 (6)	0.6643 (1)	−0.0234 (5)	3.7 (1)
N(6)	0.0672 (4)	0.6237 (1)	0.1569 (4)	2.8 (1)	C(39)	0.0050 (6)	0.6533 (1)	0.1110 (5)	3.4 (1)
N(7)	−0.2920 (4)	0.6678 (1)	0.3458 (4)	2.8 (1)	C(40)	0.2712 (6)	0.5941 (1)	−0.1676 (5)	3.6 (1)
N(8)	0.1321 (4)	0.6901 (1)	0.5878 (4)	2.57 (9)	C(41)	0.0592 (5)	0.0419 (1)	0.1737 (5)	2.9 (1)
N(9)	0.1166 (4)	0.5380 (1)	0.5596 (4)	3.0 (1)	C(42)	0.1216 (5)	0.0163 (1)	0.2689 (5)	3.0 (1)
N(10)	0.2150 (4)	0.5730 (1)	0.1009 (4)	2.78 (9)	C(43)	0.2544 (5)	0.0255 (1)	0.3000 (5)	3.1 (1)
N(11)	0.1540 (4)	0.06674 (9)	0.1526 (4)	2.50 (9)	C(44)	0.2734 (5)	0.0581 (1)	0.2272 (5)	2.6 (1)
N(12)	−0.0929 (4)	0.0899 (1)	−0.0065 (4)	3.1 (1)	C(45)	0.0700 (6)	−0.0125 (1)	0.3241 (6)	4.1 (1)
N(13)	0.3275 (4)	0.1251 (1)	0.1261 (4)	3.0 (1)	C(46)	0.1589 (6)	−0.0314 (1)	0.4112 (6)	4.7 (2)
N(14)	0.0454 (4)	0.16615 (9)	−0.0034 (4)	2.47 (9)	C(47)	0.2918 (6)	−0.0225 (1)	0.4398 (6)	4.8 (2)
N(15)	0.0096 (4)	0.1398 (1)	0.2771 (4)	2.71 (9)	C(48)	0.3448 (6)	0.0063 (1)	0.3837 (6)	3.7 (1)
N(16)	0.1819 (4)	0.1075 (1)	−0.1560 (4)	2.9 (1)	C(49)	−0.1395 (5)	0.0598 (1)	0.0354 (5)	3.1 (1)
N(17)	−0.0674 (4)	0.0389 (1)	0.1289 (4)	3.0 (1)	C(50)	−0.2688 (5)	0.0482 (1)	−0.0078 (6)	3.6 (1)
N(18)	0.3879 (4)	0.0734 (1)	0.2478 (4)	2.70 (9)	C(51)	−0.3460 (6)	0.0677 (2)	−0.1000 (6)	4.4 (1)
N(19)	−0.1038 (4)	0.19117 (9)	0.1858 (4)	2.56 (9)	C(52)	−0.2981 (6)	0.0977 (2)	−0.1477 (6)	4.3 (1)
N(20)	0.1552 (4)	0.1653 (1)	−0.2330 (4)	3.0 (1)	C(53)	−0.1727 (6)	0.1080 (1)	−0.0983 (6)	3.9 (1)
C(1)	−0.1922 (5)	0.6793 (1)	0.4235 (5)	2.6 (1)	C(54)	−0.3214 (6)	0.0159 (2)	0.0434 (7)	5.4 (2)
C(2)	−0.2174 (5)	0.7123 (1)	0.5072 (5)	2.5 (1)	C(55)	0.4208 (5)	0.1048 (1)	0.1959 (5)	2.8 (1)
C(3)	−0.0949 (5)	0.7185 (1)	0.5777 (5)	2.4 (1)	C(56)	0.5571 (5)	0.1145 (1)	0.2225 (5)	2.9 (1)
C(4)	0.0078 (5)	0.6898 (1)	0.5390 (5)	2.5 (1)	C(57)	0.5955 (5)	0.1451 (1)	0.1713 (6)	3.7 (1)
C(5)	−0.3341 (5)	0.7345 (1)	0.5230 (5)	3.1 (1)	C(58)	0.5012 (6)	0.1658 (1)	0.0985 (6)	3.8 (1)
C(6)	−0.3220 (5)	0.7642 (1)	0.6101 (6)	3.7 (1)	C(59)	0.3698 (5)	0.1551 (1)	0.0800 (5)	3.4 (1)
C(7)	−0.1984 (6)	0.7704 (1)	0.6782 (6)	3.7 (1)	C(60)	0.6571 (5)	0.0931 (1)	0.3081 (6)	3.7 (1)
C(8)	−0.0821 (5)	0.7478 (1)	0.6653 (5)	3.1 (1)	C(61)	−0.0496 (5)	0.1898 (1)	0.0626 (5)	2.6 (1)
C(9)	−0.2944 (5)	0.6349 (1)	0.2814 (5)	2.9 (1)	C(62)	−0.0853 (5)	0.2176 (1)	−0.0348 (5)	2.7 (1)
C(10)	−0.4083 (5)	0.6290 (1)	0.1919 (5)	3.3 (1)	C(63)	−0.0082 (5)	0.2108 (1)	−0.1551 (5)	2.8 (1)
C(11)	−0.4273 (5)	0.5955 (1)	0.1442 (6)	3.7 (1)	C(64)	0.0731 (5)	0.1777 (1)	−0.1342 (5)	2.7 (1)
C(12)	−0.3319 (6)	0.5692 (1)	0.1805 (6)	3.8 (1)	C(65)	−0.1772 (5)	0.2464 (1)	−0.0202 (5)	3.4 (1)
C(13)	−0.2209 (5)	0.5774 (1)	0.2614 (5)	3.2 (1)	C(66)	−0.1864 (6)	0.2683 (1)	−0.1315 (6)	3.8 (1)
C(14)	−0.5099 (6)	0.6576 (2)	0.1566 (6)	5.0 (2)	C(67)	−0.1106 (6)	0.2612 (1)	−0.2533 (6)	3.8 (1)
C(15)	0.2417 (5)	0.6658 (1)	0.5596 (5)	2.6 (1)	C(68)	−0.0189 (5)	0.2323 (1)	−0.2677 (5)	3.3 (1)
C(16)	0.3671 (5)	0.6726 (1)	0.6301 (5)	2.9 (1)	C(69)	−0.0781 (5)	0.1686 (1)	0.2914 (5)	2.7 (1)
C(17)	0.4828 (5)	0.6504 (1)	0.6043 (5)	3.3 (1)	C(70)	−0.1484 (5)	0.1770 (1)	0.4188 (5)	3.0 (1)
C(18)	0.4721 (5)	0.6219 (1)	0.5148 (5)	3.2 (1)	C(71)	−0.1264 (5)	0.1560 (1)	0.5292 (5)	3.3 (1)
C(19)	0.3473 (5)	0.6164 (1)	0.4517 (5)	3.2 (1)	C(72)	−0.0351 (6)	0.1272 (1)	0.5170 (5)	3.3 (1)
C(20)	0.3762 (6)	0.7031 (1)	0.7323 (6)	4.3 (1)	C(73)	0.0290 (5)	0.1202 (1)	0.3896 (5)	3.1 (1)
C(21)	0.1589 (5)	0.5413 (1)	0.4329 (5)	2.7 (1)	C(74)	−0.2485 (6)	0.2083 (1)	0.4325 (6)	3.8 (1)
C(22)	0.2639 (5)	0.5156 (1)	0.3713 (5)	2.8 (1)	C(75)	0.2167 (5)	0.1318 (1)	−0.2428 (5)	2.9 (1)
C(23)	0.2883 (5)	0.5250 (1)	0.2373 (5)	3.0 (1)	C(76)	0.3069 (5)	0.1242 (1)	−0.3578 (5)	3.5 (1)
C(24)	0.2020 (5)	0.5571 (1)	0.2165 (5)	2.8 (1)	C(77)	0.3509 (6)	0.0905 (1)	−0.3860 (5)	3.9 (1)
C(25)	0.3323 (6)	0.4869 (1)	0.4275 (5)	3.8 (1)	C(78)	0.3117 (6)	0.0650 (1)	−0.3003 (6)	3.9 (1)
C(26)	0.4272 (6)	0.4684 (1)	0.3408 (6)	4.4 (1)	C(79)	0.2285 (5)	0.0748 (1)	−0.1866 (5)	3.4 (1)
C(27)	0.4504 (6)	0.4773 (1)	0.2047 (6)	4.4 (1)	C(80)	0.3458 (6)	0.1520 (2)	−0.4504 (6)	4.9 (2)
C(28)	0.3809 (6)	0.5059 (1)	0.1506 (6)	3.8 (1)	C(M)	0.3320 (7)	0.2469 (2)	−0.1764 (7)	6.5 (2)
C(29)	0.0170 (5)	0.5586 (1)	0.6324 (5)	3.0 (1)					

[a] Anisotropically refined atoms are given in the form of the isotropic equivalent thermal parameter defined as $^4/_3[a^2B_{11} + b^2B_{22} + c^2B_{33} + ab(\cos\gamma)B_{12} + ac(\cos\beta)B_{13} + bc(\cos\alpha)B_{23}]$.

product but with loss of some deuterium on the pyridyl ring. The reaction was repeated with deuterated amide, giving the desired retention of pyridyl deuterium. Subsequent exchange of amino hydrogens with water was not of importance to further reactions.

Phthalonitrile-d_4. This product was prepared from *o*-xylene-d_{10} by permanganate oxidation to the phthalic-d_4 acid and subsequent conversion to the nitrile. The procedure was similar to that outlined for the *tert*-butyl derivative.

Crystal Structure Analysis. The crystal used for the structure was grown from CH_2Cl_2 by slow evaporation. Crystal data at −100 °C: space group $P\bar{1}$, a = 9.643 (2), b = 38.930 (9), c = 9.539 (2) Å; α = 92.716 (2), β = 90.556 (2), γ = 86.574 (2)°; V = 3570 Å³; λ = 0.710 69 Å; four complex and two CH_2Cl_2 molecules per unit cell; linear absorption coefficient 5.12 cm⁻¹; calculated density 1.395 g cm⁻³.

Data were collected to a Syntex P3 diffractometer using Mo Kα radiation. A total of 5455 reflections were used in the refinement of 946 variables. All non-hydrogen atoms were refined with anisotropic thermal parameters, and hydrogen atoms were fixed. The model converged with R = 0.044 and R_w = 0.044. Figure 1 presents average values of important bond distances and angles. Figure 2 presents a stereoview of molecule 1. Table VII presents the final positional parameters for the non-hydrogen atoms. Further details of the X-ray analysis and tables of thermal parameters, general temperature factor expressions, selected bond distances and angles, and observed and calculated structure factors have been deposited as supplementary material. Additional views of the structure have also been placed there.

Acknowledgment. We wish to thank M. A. Cushing, R. M. Swiatek, L. Lardear, G. Watunya, and F. N. Schoch for their skilled technical assistance. This work was supported by a generous instrument grant from the National Institute of Health (Grant No. RR00292) to Carnegie-Mellon University. We thank A. A. Bothner-by and K. S. Lee of Carnegie-Mellon University for their help with the 600-MHz spectra.

Registry No. 2, 33252-26-5; $Co(BPI)_2$, 14911-23-0; $Co(3\text{-}MeBPI)_2$, 79062-08-1; $Co(4\text{-}MeBPI)_2$, 78065-32-4; $Co(5\text{-}MeBPI)_2$, 79062-10-5; $Co(4\text{-}t\text{-}BuBPI)_2$, 79062-02-5; $Ni(BPI)_2$, 15134-62-0; $Ni(3\text{-}MeBPI)_2$,

82090-98-0; Ni(4-MeBPI)$_2$, 78065-33-5; Ni(5-MeBPI)$_2$, 87802-48-0; Ni(4-*t*-BuBPI)$_2$, 87802-49-1; Fe(BPI)$_2$, 79062-05-8; Fe(3-MeBPI)$_2$, 79062-04-7; Fe(4-MeBPI)$_2$, 78065-31-3; Fe(5-MeBPI)$_2$, 87802-50-4; Fe(4-*t*-BuBPI)$_2$, 87802-51-5; Mn(3-MeBPI)$_2$·$^1/_2$CH$_2$Cl$_2$, 87802-52-6; Zn(BPI)$_2$, 87802-53-7; 4-*tert*-butylphthalic acid, 14236-13-6; 4-tert-butylphthalonitrile, 32703-80-3; 2-aminopyridine-d_4, 87802-54-8; phthalonitrile-d_4, 69299-71-4.

Supplementary Material Available: Details of the crystal structure analysis, space group, and unit cell data, listings of positional and thermal parameters and selected individual bond distances, angles, torsional angles, and least-squares planes, additional perspective and stereoscopic views of the molecules, and a table of structure factor amplitudes (71 pages). Ordering information is given on any current masthead page.

Contribution from the Department of Chemistry, University of Arizona, Tucson, Arizona 85721, and Lehrstuhl für Anorganische Chemie I, Ruhr Universität Bochum, 4630 Bochum Querenburg, Federal Republic of Germany

^{95}Mo NMR Studies of Dioxo, Oxo–Sulfido, Oxo–Selenido, and Disulfido Complexes of Molybdenum(VI)

MARTIN MINELLI, JOHN H. ENEMARK,* KARL WIEGHARDT, and MANFRED HAHN

Received April 21, 1983

The ^{95}Mo NMR spectra of a number of Mo(VI) complexes with the general formula MoXY[ONHR]$_2$ and MoXY[ONR$_2$]$_2$ (X = O, S, Se; Y = O, S; R = CH$_3$, C$_2$H$_5$, C(CH$_3$)$_3$, CH$_2$C$_6$H$_5$; R$_2$ = C$_5$H$_{10}$) have been measured. Change of the terminal groups from oxygen to sulfur to selenium causes deshielding of the molybdenum nucleus in the order O < S < Se. A narrowing of the line width accompanies this deshielding. Bulky R groups also seem to have some deshielding effect. The quantitative conversion of the dioxo (MoO$_2$) complexes to the corresponding monooxo–monosulfido (MoOS) and disulfido (MoS$_2$) complexes by reaction with [(CH$_3$)$_3$Si]$_2$S was followed by ^{95}Mo NMR. Under similar conditions MoOSe[ONR$_2$]$_2$ was converted to MoOS[ONR$_2$]$_2$, MoS$_2$[ONR$_2$]$_2$, and several other species.

Introduction

Recently we have shown that low-symmetry, six-coordinate Mo(VI) complexes containing the $[MoO_2]^{2+}$ unit can be conveniently studied by ^{95}Mo NMR.[1,2] Another important group of $[MoO_2]^{2+}$ complexes are the Mo(VI) complexes of structure **1** that result from the reaction of substituted hydroxylamines with molybdate.[3] Our special interest in these complexes stems from the fact that their terminal oxo groups can be replaced by terminal sulfido and terminal selenido groups. Such complexes are relevant to understanding the molybdenum site of the oxidized form of xanthine oxidase. The molybdenum center of the active form of this enzyme is believed to contain a Mo(VI) atom with one terminal oxo and one terminal sulfido group (MoOS), whereas the inactive, cyanolyzed form of the enzyme is postulated to have two terminal oxo groups (MoO$_2$).[4] A ^{95}Mo NMR study of complexes of type **1** in which the terminal oxo groups can be replaced by sulfido groups is therefore an important prerequisite to future ^{95}Mo NMR studies of molybdenum in enzymes and their cofactors.[5] The ^{95}Mo NMR spectra for several type **1** complexes appeared while this work was in progress.[6] Here we present results for additional examples and show that the formation and the interconversions of the terminal O, S, and Se groups in type **1** complexes can be followed by ^{95}Mo NMR.

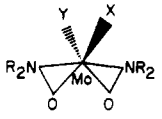

1

Experimental Section

The complexes were synthesized as previously described.[3] The ^{95}Mo NMR data were obtained on a Bruker WM250 NMR spectrometer. A 10-mm molybdenum probe (16.3 MHz) was used. A delay of 200 μs prior to acquisition was used to reduce the effects of probe ringing.

Table I. ^{95}Mo NMR Data

compd	chem shift,[a] ppm	line width, Hz
MoO$_2$[ONH(CH$_3$)]$_2$	−219	200
MoO$_2$[ONH(C(CH$_3$)$_3$)]$_2$	−218	150
MoO$_2$[ON(CH$_3$)$_2$]$_2$	−165	120
MoO$_2$[ON(C$_2$H$_5$)$_2$]$_2$	−169	160
MoOS[ON(C$_2$H$_5$)$_2$]$_2$	+544	140
MoOSe[ON(C$_2$H$_5$)$_2$]$_2$	+865	120
MoS$_2$[ON(C$_2$H$_5$)$_2$]$_2$	+1234	100
MoO$_2$[ONC$_5$H$_{10}$]$_2$	−184	160
MoOS[ONC$_5$H$_{10}$]$_2$	+531	100
MoOSe[ONC$_5$H$_{10}$]$_2$	+855	70
MoS$_2$[ONC$_5$H$_{10}$]$_2$	+1219	70
MoO$_2$[ON(CH$_2$C$_6$H$_5$)$_2$]$_2$	−161	260

[a] Measured at room temperature in DMF, concentration 0.4 M; if less soluble, saturated; chemical shifts relative to 2 M Na$_2$MoO$_4$ in H$_2$O at pH 11. The estimated uncertainty of the chemical shifts is ±1 ppm.

A 2 M Na$_2$MoO$_4$ solution at pH 11 served as external standard. All solvents were dried prior to use. In the case of the oxo–selenido complexes the NMR spectra were measured in sealed 10-mm NMR tubes under nitrogen; in the other cases regular 10-mm NMR tubes were used.

In Situ Thiolation Reactions. MoO$_2$[ON(C$_2$H$_5$)$_2$]$_2$ (1.5 m Mol) was dissolved in 2.5 mL of dry DMF under nitrogen in a 10-mm sealed screw top NMR tube (Wilmad) and the ^{95}Mo NMR spectrum measured. An equimolar amount of [(CH$_3$)$_3$Si]$_2$S (Fluka Chemical

* To whom correspondence should be addressed at the University of Arizona.

(1) Christensen, K. A.; Miller, P. E.; Minelli, M.; Rockway, T. W.; Enemark, J. H. *Inorg. Chim. Acta* **1981**, *56*, L27.
(2) For a complete list of ^{95}Mo NMR studies see: Minelli, M.; Hubbard, J. L.; Christensen, K. A.; Enemark, J. H. *Inorg. Chem.* **1983**, *22*, 2652.
(3) (a) Wieghardt, K.; Holzbach, W.; Weiss, F.; Nuber, B.; Prikner, B. *Angew. Chem., Int. Ed. Engl.* **1979**, *18*, 548. (b) Wieghardt, K.; Hahn, M.; Weiss, J.; Swiridoff, W. *Z. Anorg. Allg. Chem.*, in press.
(4) Cramer, S. P.; Wahl, R.; Rajagopalan, K. V. *J. Am. Chem. Soc.* **1981**, *103*, 7721.
(5) Johnson, J. L. In "Molybdenum and Molybdenum Containing Enzymes"; Coughlan, M. P., Ed.; Pergamon Press: Oxford, 1980; p 345.
(6) Gheller, S. F.; Hambley, T. W.; Traill, P. R.; Brownlee, R. T. C.; O'Connor, M. J.; Snow, M. R.; Wedd, A. G. *Aust. J. Chem.* **1982**, *35*, 2183.

0020-1669/83/1322-3952$01.50/0